Journal of Power Sources 201 (2012) 49–58

Contents lists available at SciVerse ScienceDirect

Journal of Power Sources

journal homepage: www.elsevier.com/locate/jpowsour

Preparation and characterization of Ce- and La-doped $Ba_2In_2O_5$ as candidates for intermediate temperature (100–500 °C) solid proton conductors

Jasna Jankovic[a,b,*], David P. Wilkinson[a,b,**], Rob Hui[b]

[a] Department of Chemical and Biological Engineering, University of British Columbia, Vancouver, BC, Canada V6T 1Z4
[b] Institute for Fuel Cell Innovation, National Research Council Canada, Vancouver, BC, Canada V6T 1W5

ARTICLE INFO

Article history:
Received 26 August 2011
Received in revised form 28 October 2011
Accepted 30 October 2011
Available online 6 November 2011

Keywords:
$Ba_2In_2O_5$
Perovskites
Brownmillerites
Electrical conductivity
Proton conductivity
Fuel cells

ABSTRACT

Five different compositions of brownmillerite materials, Ce- and La-doped, and undoped $Ba_2In_2O_5$ were synthesized via the solid-state reaction and the glycine-nitrate combustion process. Properties of the materials were characterized using XRD, HR-TEM, and TGA/DSC techniques. Conductivity measurements by AC impedance spectroscopy, performed in air and hydrogen-containing atmospheres, in the temperature range from 100 °C to 500 °C, were correlated to the properties of the materials and revealed the effects of dopant, microstructure, temperature and atmosphere on the total electrical conductivity of the materials. All compositions showed low conductivity in air. In hydrogen-containing atmospheres, while Ce- and La-doped $Ba_2In_2O_5$ showed low conductivity (4×10^{-6}–3×10^{-6} S cm^{-1} at 500 °C), undoped $Ba_2In_2O_5$ demonstrated a surprisingly high conductivity (between 0.02 S cm^{-1} and 0.7 S cm^{-1} in the temperature range from 300 °C to 500 °C), especially samples produced by the glycine-nitrate process. This finding creates potential opportunity for using $Ba_2In_2O_5$ as a proton-conductive material in intermediate temperature fuel cells.

1. Introduction

In recent years, more intense research has taken place to develop intermediate temperature fuel cells (100–500 °C) since they combine the advantages of both high and low temperature fuel cells [1–8]. One of the major approaches to achieve this goal involves searching for new electrolyte materials with a sufficiently high ionic conductivity in that temperature range. Proton-conducting ceramics attract significant attention due to their potential for proton conduction below 500 °C. Proton conduction in ceramic materials has been reported before [9–12]. Some doped perovskite-type oxides ABO_3 (e.g., $BaCeO_3$, $SrCrO_3$, $SrZrO_3$) and related brownmillerite-type oxides (e.g., $Ba_2In_2O_5$) have been reported to show mixed oxygen ion, electron and proton conduction, with predominant oxygen ion conduction at high temperatures (above 500 °C) and predominant protonic conduction at low temperatures (below 500 °C). The mechanism of ions (oxygen or proton) incorporation in perovskite and brownmillerite ceramics in presence of oxygen, water vapour or hydrogen has been suggested elsewhere [11–14]. In general, the ion incorporation and the conductivity of these materials is due to the presence of oxygen vacancies, which are usually formed by doping the ideal perovskite $A^{2+}B^{4+}O_3{}^{2-}$ with lower-valent metal M^{3+} ions. In order to keep the charge balance, oxygen leaves the structure, forming vacancies. Special cases of the acceptor-doped perovskites are the brownmillerite-structured oxides, such as $Ba_2In_2O_5$, where B^{4+} ions are completely substituted by lower-valent metal ions, M^{3+} [10,11,15]. At lower temperatures (e.g., up to 925 °C for $Ba_2In_2O_5$) the oxygen vacancies are ordered in parallel tetrahedral oxygen vacancy layers, alternating with octahedral perovskite layers [16]. At a certain characteristic temperature for these types of materials, the so-called transition order–disorder temperature (T_d), oxygen vacancies start to distribute randomly. With further heating, the vacancies become completely disordered so that the structure reverts to that of a highly defective cubic perovskite [10,11,17]. The material exhibits a dramatic increase in electrical conductivity as the "trapped" oxygen vacancies become partially disordered. For $Ba_2In_2O_5$ the transition order–disorder temperature is $T_d \approx 925$ °C [11]. In order to obtain enhanced conductivity in the intermediate temperature range, it is necessary to reduce the T_d and stabilize the disordered phase at lower temperatures. The substitution of barium (II) or indium (III) in $Ba_2In_2O_5$ with other cations has been reported to lead to the reduction of T_d and the improvement of total conductivity at lower temperatures (below 900 °C) [18–21]. Based on the results reported in these studies it is expected to be beneficial to

* Corresponding author at: Department of Chemical and Biological Engineering, University of British Columbia, Vancouver, BC, Canada V6T 1Z4.
Tel.: +1 778 331 3205; fax: +1 604 415 7291.
** Corresponding author at: Department of Chemical and Biological Engineering, University of British Columbia, Vancouver, BC, Canada V6T 1Z4.
Tel.: +1 604 822 4888; fax: +1 604 822 6003.
E-mail addresses: jjankovic@chbe.ubc.ca (J. Jankovic), dwilkinson@chbe.ubc.ca (D.P. Wilkinson).

0378-7753/$ – see front matter © 2011 Elsevier B.V. All rights reserved.
doi:10.1016/j.jpowsour.2011.10.104

Table 1
List of prepared samples with compositions and acronyms used.

Composition	Acronym	Atomic ratio obtained by TEM-EDS
$Ba_2In_2O_5$	BIO	Ba/In = 0.94 (±0.04)
$Ba_2In_{1.5}Ce_{0.5}O_{5.25}$	BIC	Ba/In = 1.36 (±0.03); Ba/Ce = 4.04 (±0.05)
$Ba_2In_{1.5}Ce_{0.25}La_{0.25}O_{5.125}$	BICL025	Ba/In = 1.35 (±0.01); Ba/Ce = 7.73 (±0.03); Ba/La = 8.74 (±0.03)
$Ba_2In_1Ce_{0.5}La_{0.5}O_{5.25}$	BICL05	Ba/In = 1.95 (±0.04); Ba/Ce = 3.72 (±0.02); Ba/La = 4.10 (±0.02)
$Ba_2In_{1.5}La_{0.5}O_5$	BIL	Ba/In = 1.38 (±0.04); Ba/La = 3.73 (±0.05)

substitute indium (III) in $Ba_2In_2O_5$ by cerium (IV) and lanthanum (III) cations, in order to lower the order–disorder transition temperature and hence increase electrical conductivity of these materials at lower temperatures.

In this work our goal was to prepare and characterize some new compositions of Ce- and La-doped $Ba_2In_2O_5$, along with some previously investigated Ce-doped and undoped $Ba_2In_2O_5$ for comparison. A particularly important aspect of this work was to study the electrical conductivity of these materials in hydrogen-containing atmospheres and in the temperature range from 100 °C to 500 °C, conditions that have not been studied much or at all for some of these types of materials. These conditions are important in order to determine potential proton conductive ceramic materials for application in the intermediate temperature range (100–500 °C). Another important aspect of this study was to correlate the properties of the investigated ceramics, especially the grain (crystallite) size and the transition order–disorder temperature, with the electrical conductivity of the materials. The materials in this work were produced by two different methods consisting of the glycine-nitrate combustion process or the solid-state reaction. After the materials characterization, the effect of dopants, microstructure, temperature and atmosphere on electrical conductivity was investigated. Based on the results, a candidate for further, more detailed study on proton conductivity was chosen.

2. Experimental procedure

2.1. Materials preparation

Samples of $Ba_2In_{2-x-y}Ce_xLa_yO_{5+x/2}$ ($x = 0.25$ and 0.5; $y = 0.25$ and 0.5) were synthesized via the glycine-nitrate combustion process (GNP) and solid-state reaction (SS). The level of dopants was chosen to be 0.5 in total ($x + y = 0.5$). Based on the previous reported studies by Hui et al. [12], Niwa et al. [18] and Mitamura et al. [21] it was expected that at this higher level of doping the disordered structure of the material would be stabilized at lower temperatures, and hence electrical conductivity improved. For comparison purposes, non-doped $Ba_2In_2O_5$ was also synthesized by both procedures. The elemental analysis of the powder samples was done by TEM – energy-dispersive X-ray spectroscopy (EDS). All compositions and their acronyms are listed in Table 1.

2.1.1. Glycine-nitrate combustion process (GNP)

The glycine-nitrate combustion process was used to produce samples of all five compositions. Glycine (NH_2CH_2COOH) (Alfa Aesar), which serves as a complexing agent and a fuel, was dissolved in distilled water. Ba-acetate ($Ba(OOCCH_3)_2$), Ce-, La- and In-nitrate ($Ce(NO_3)_3{\cdot}6H_2O$, $La(NO_3)_3{\cdot}6H_2O$ and $In(NO_3)_3{\cdot}1.5H_2O$, respectively), all from Alfa Aesar were added in their appropriate stoichiometric ratio. Glycine was added in the amount to achieve a glycine/total-nitrates ratio of 5. Such a high glycine/nitrate ratio was necessary in order to prevent precipitation of Ba-acetate. The solution was then heated with stirring in a glass beaker for 2 h until all salts were fully dissolved. The solution was then transferred into a 5 l stainless steel pot and heated on a hot plate until the viscous liquid started bubbling and forming foam. The combustion happened slowly, forming a dark, very porous ash of partially reacted precursors. Additional calcining in a crucible at a high temperature (in the range of 1100–1500 °C) for 6 h was needed to achieve a pure crystalline phase. The powders were compacted by a lab spoon in the crucible to enable better material contact. To determine the temperature at which the desired brownmillerite phase was formed, samples of all five compositions were calcined to 1100 °C, 1200 °C, 1300 °C, 1400 °C and 1500 °C for 6 h. The phase obtained after calcination at each temperature was determined by X-ray diffraction at room temperature.

2.1.2. Solid-state reaction process (SS)

Stoichiometric quantities of nitrate precursors were ball-milled in ethanol (94–96%, Alfa Aesar) overnight. All samples were subsequently heated to 150 °C overnight to release the water. The dried samples were ground into fine powders, pressed into pellets (7 MPa pressure was used) to achieve better contact, and calcined to a high temperature (in the range of 1100–1500 °C) for 10 h when the brownmillerite structure is formed. Grinding, pressing and calcining steps had to be repeated two times in order to achieve a pure phase.

2.2. Materials characterization

As-calcined powder samples prepared by both the solid-state and GNP methods were investigated by X-ray powder diffraction at room temperature on a Bruker AXS D8 X-ray diffractometer with a CuKα source. $Ba_2In_2O_5$, as a well investigated composition in the literature [10,11,18] was used as a reference. Grain size of the prepared powders was determined using the Scherrer [22] equation based on the peak broadening in the X-ray patterns.

During the experimental work on the five compositions, it was noticed that they show some instability in humid atmospheres. A short study was performed to investigate this. The samples placed in a controlled atmosphere furnace were exposed to air from a humidifier (Setaram Wetsys) with relative humidity of 50% and 90% and temperatures of 25 °C, 50 °C, and 70 °C for 24 h. The effect of humidity at higher temperatures in the range between 100 °C and 500 °C, which could not be achieved by the Wetsys humidifier, was investigated by flowing 100 sccm air through a bubbler at room temperature and over the tested samples in a closed tube furnace. The humidification achieved was approximately 3 mol%. Composition of the samples after exposure to humidity was determined by XRD.

Thermal properties of the as-synthesized powders were evaluated using a SETARAM Setsys Evolution thermal analysis instrument. The thermogravimetric analysis (TGA) was performed to measure the weight change of the samples as a function of temperature, while differential scanning calorimetry (DSC) was used to record thermal effects related to the order–disorder transitions and other changes in the material. TGA and DSC tests were carried out in air in an alumina crucible up to 1000 °C with a heating and cooling rate of 5 °C min^{-1}. X-ray diffraction measurements were performed before and after the thermogravimetric analysis, to identify any phase change during heating.

Phase changes and order–disorder transition temperatures were also confirmed by temperature-profile X-ray diffraction. Each powder sample with a starting brownmillerite structure, confirmed by XRD at room temperature, was heated consecutively to 400 °C, 600 °C, 800 °C and 1000 °C. After 3 h of equilibration at each temperature XRD was measured and heating to a higher temperature continued.

Table 2
Summary of the sintering temperatures and obtained properties for the testing pellets for conductivity measurements. Testing pellets were prepared from the powders produced by the glycine-nitrate process (GNP) and the solid-state process (SS), pressed in a die to 150 MPa and sintered. All compositions have the brownmillerite structure.

Sintered sample (compos.-method)	Sintering T (6 h) (°C)	Grain size (nm)	Porosity (%)
BIO-GNP	1350	42	18
BIO-SS	1400	57	20
BIC-GNP	1350	42	20
BIC-SS	1400	60	21
BICL025-GNP	1300	44	20
BICL025-SS	1300	61	19
BIL-GNP	1350	42	20
BIL-SS	1400	65	20

2.3. Preparation of samples for conductivity measurements

Pellets for conductivity measurement were prepared from powders made by the GNP process or the solid-state reaction. 2 wt% of PVB binder (Richard E. Mistler Inc.) dissolved in ethanol (10 wt% solution) was added to the powders to help prepare stronger green body of the pressed pellets. The powders were pressed in a 20 mm die using a pneumatic press under 150 MPa pressure. The pellets were sintered at different temperatures, depending on the composition and powder preparation method. A short study was performed to determine the appropriate sintering temperatures for the samples. Table 2 shows a summary of the sintering temperatures and achieved pellet properties for all prepared materials. BICL05 was impossible to make into pellets, as the samples always fractured into pieces. Hence, this material was not tested for conductivity. The final phase of the sintered samples was confirmed by the X-ray diffraction and the final grain size of the pellets was determined using the Scherrer equation.

An attempt was made to confirm these results by SEM. Sintered pellets made by the GNP or the solid-state process were polished (final polishing was with a 1 μm cloth) and etched using 0.3% HNO_3 for 1 min. Cross-section of the pellets was observed using a high resolution SEM (FEI DualBeam Strata 235) in order to confirm the grain size of the samples.

The density of the pellets was determined by the Archimedes principle in ethanol (94–96%, Alfa Aesar, $\rho_{20\,^\circ C} = 0.7893\ g\,cm^{-3}$). Fully dense samples could not be prepared and the lowest total porosity obtained was between 16 and 20% (with ~4% open porosity). Samples with a similar total porosity of about 20% and open porosity of 4% were used for the conductivity measurements in order to minimize the effect of the porosity factor on the conductivity results. At this low open porosity, it is expected that measured conductivity is mainly due to the bulk conductivity and not due to the surface diffusion. The microstructures of the sintered samples were examined using an Hitachi S-3500N scanning electron microscope (SEM). Pt paste was applied on both sides of the sintered samples to act as contact electrodes.

2.4. Conductivity measurements

Conductivity measurements for all five compositions made by both the GNP and the solid-state process were performed in air and hydrogen-containing atmospheres by AC impedance spectroscopy, using an impedance analyzer (IM6 by Zahner Electrinks), in a frequency range from 100 mHz to 8 MHz and with an amplitude of 50 mV, in the temperature range from 100 °C to 500 °C. At least three measurements with fresh samples were performed for all compositions and under all conditions. Samples were held at each temperature for 3 h to achieve equilibrium, and impedance measurements were performed every 30 min over the 3 h. The electrical conductivities were assessed in two different atmospheres: air (supplied from the atmosphere and dried to contain up to 15 ppm) and a hydrogen/nitrogen mixture (50% H_2/50% N_2). Nitrogen and hydrogen used in the experiments (Praxair) contained maximum 3 ppm (vol) of water and maximum 3 ppm oxygen (in N_2) and 1 ppm oxygen (in H_2). The ceramic samples were exposed to the same atmosphere on both sides with a gas flow rate of 100 sccm. The temperature and gas flow rate were programmed using an AMEL 7902 test setup. Before the actual testing, preliminary measurements were performed for all tested compositions to determine what part of the impedance spectra was associated with the material bulk resistivity, and what part with the electrode charge transfer. These experiments involved testing samples with different electrodes (Pt vs. Au) in both testing atmospheres and at each testing temperature. The response resulted in differences in the AC impedance part associated to the electrode contribution and enabled determination of the resistance due only to the material.

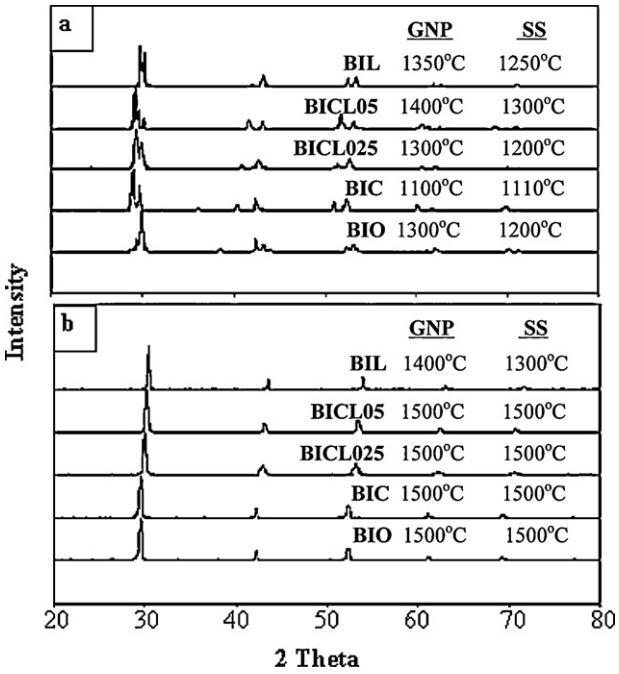

Fig. 1. X-ray powder diffraction spectra for five different compositions: (a) orthorhombic brownmillerite structure; (b) cubic perovskite structure. The temperatures needed to achieve a particular phase are given for both the GNP and the solid-state (SS) method of preparation.

3. Experimental results and discussion

3.1. Structure and stability

Typical X-ray diffraction patterns of the prepared powder samples for all five compositions are given in Fig. 1a and b. As shown in figure, the samples could be indexed to either an orthorhombic brownmillerite or cubic perovskite structure, depending on the calcining temperature. Comparable scans were obtained for powders produced by the two different methods, the GNP and the solid-state method. However, the calcining temperatures needed to achieve particular phases for the powders produced by the GNP method or by the solid-state method were different, as shown in the figure. Lower calcining temperatures for the solid-state powders are probably due to the closer contact of particles during pneumatic pressing in the preparation stage (which was not present for the GNP powders) and, hence, better heat and material transport.

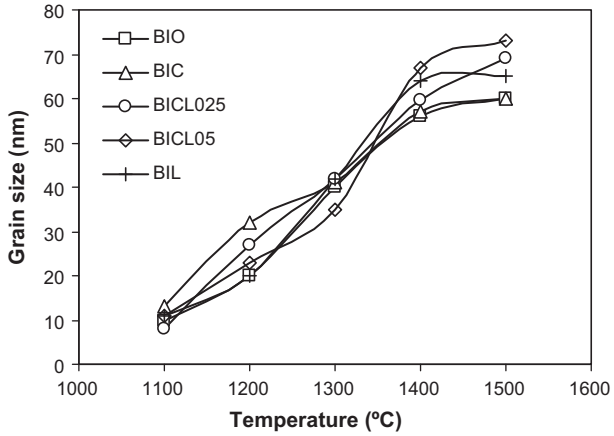

Fig. 2. Grain size as a function of calcining temperature for powders produced by the GNP process.

Scherrer equation given below was used to calculate grain size of the powder samples made by the two different methods based on the peak broadening in the X-ray patterns. The grain size D is given by

$$D = \frac{0.89\lambda}{\sqrt{W^2 - W_0^2}\,\cos\theta} \quad (1)$$

where λ is the wavelength of the Cu source used in XRD, W is the peak width at half of the diffraction peak height (peak with the highest intensity was used, but also compared with several lower intensity peaks), W_0 is the instrumental broadening, and θ is the half value of the 2θ angle of diffraction. The instrumental broadened profile was obtained from the measurement of the standard sample NIST SRM 1976 Alumina (National Institute of Standards and Technology – NIST, USA).

Fig. 2 shows the effect of calcining temperature on the grain size of the powders produced by the GNP method. Powders produced by the GNP method, right after combustion and before additional calcining, had a starting grain size of about 10 nm. The starting grain size of powders made by the solid-state reaction was determined to be around 40 nm. Further heating to higher temperatures gave similar results for grain size as for the GNP powders.

The TEM image in Fig. 3 shows an agglomeration of crystalline particles of a BIC powder produced by the GNP process.

Our short study on stability of the prepared materials in humid atmospheres showed that in most cases the materials were not stable if exposed to the flow of humidified air at RH = 90% and temperatures between 25 °C and 70 °C. The materials mostly decomposed into $BaCO_3$ and $In(OH)_3$. Under a lower humidification of RH = 50% only BIO decomposed, while the other compositions showed higher stability at all temperatures. Instability of the materials at high humidification levels, such as during fuel cell operation, is an issue if these materials are to be used as fuel cell electrolytes. The stability would need to be improved by possibly doping the materials with a stabilizing dopant. When the samples were exposed to a low humidification of 3 mol% steam in air flow at temperatures from 100 °C to 500 °C, X-ray diffraction of the samples did not show any change in the composition. This humidity level corresponds to the composition of the feeding stream for the solid oxide fuel cells.

3.2. Temperature-profile XRD

It has been reported [11,23,24] that, at a certain temperature, $Ba_2In_2O_5$-based materials undergo a phase transition from orthorhombic brownmillerite structure with ordered oxygen vacancies, to a disordered cubic perovskite structure. The temperature at which this change happens is the earlier mentioned transition order–disorder temperature, T_d, and is also related to the change in conductivity of the materials. In order to investigate this change for all five compositions in the present study, temperature-profile XRD measurements were carried out. Fig. 4a and b shows the changing X-ray diffraction patterns of the powder structures achieved with temperature for the BIO and BIC samples. Structures achieved with temperature for all five compositions are listed in Table 3. Samples prepared by both the GNP

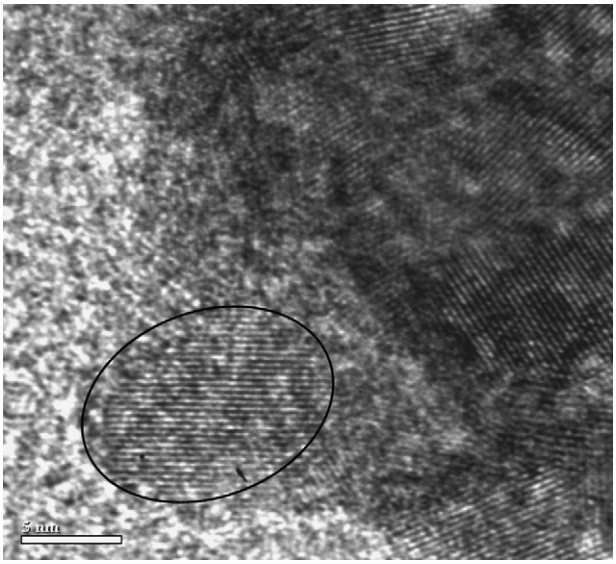

Fig. 3. TEM image of as-synthesized BIC powder prepared by the GNP process – a selected grain with crystal fringe (scale 5 nm).

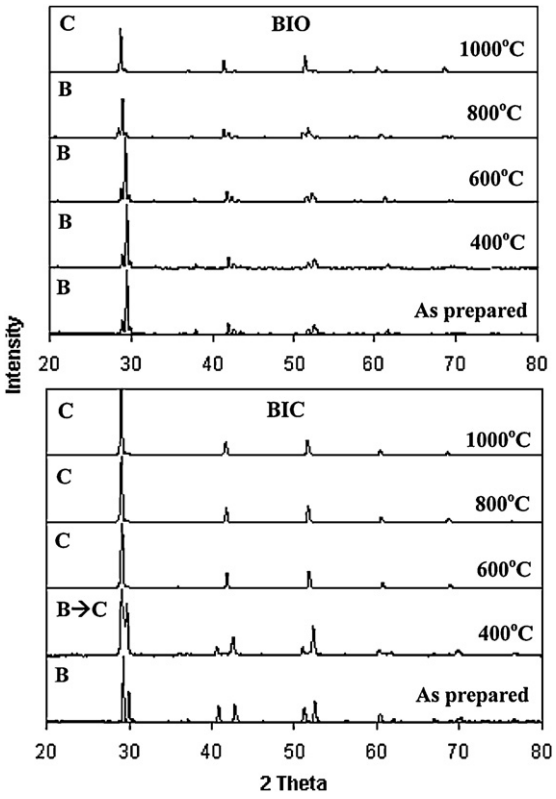

Fig. 4. Temperature-profile XRD of BIO and BIC sample both with a starting brownmillerite structure. Note: B – brownmillerite structure; C – cubic structure.

Table 3
Temperature-profile XRD measurement results showing the change in structure with temperature. Order–disorder transition temperature were determined from DSC data or estimated from DSC, XRD and TGA.

T(°C)	RT	400	600	800	1000	T_d (°C) based on DSC
BIO	B	B	B	B	C	925
BIC	B	B → C	C	C	C	480[a]
BICL025	B	C	C	C	C	410
BICL05	B	C	C	C	C	430
BIL	B	C	C	C	C	420[a]

B – brownmillerite structure; C – cubic structure.
[a] Estimated based on the temperature-profile XRD, TGA and DSC data.

and solid-state method showed the same behavior. BIO, with a starting brownmillerite structure transformed to a cubic perovskite structure between 800 °C and 1000 °C, in agreement with 925 °C based on the literature [10,11,18]. BIC starts its change to a cubic structure at a lower temperature of around 400 °C, while BICL025, BICL05 and BIL almost completely change to a cubic structure at around 400 °C. In general, the Ce- and La-doped $Ba_2In_2O_5$ experienced transition from an ordered brownmillerite structure to a disordered cubic structure at lower temperatures (T_d) compared to undoped $Ba_2In_2O_5$. This finding confirms the hypothesis that introduction of Ce and La into the $Ba_2In_2O_5$ structure would decrease the order–disorder temperature of the material [18,19,21]. TGA and DSC results in the following section give us additional information on this effect.

3.3. Thermogravimetric analysis and DSC

Figs. 5 and 6 represent the TGA and DSC results for all five compositions made by the GNP process and, for comparison, the TGA result obtained for a BIO sample made by the solid-state reaction. For the case of BIO, similar results were obtained for samples made by the GNP and solid-state reaction process. A small difference was observed in the TGA result, where GNP sample showed somewhat larger initial weight loss, compared to the solid-state sample. All other compositions prepared by the GNP and the solid-state process had similar TGA and DSC results, even without a significant difference in the initial weight loss. Therefore, results for BIC, BIL, BICL025 and BICL05 made by the solid-state reaction are not shown here. For all samples TGA reveals a significant weight loss in the 300–400 °C temperature range. An endothermic peak in the DSC curves is associated with this change, as shown in Fig. 6. As reported in the literature [12,25,26] this change is related to the loss of H_2O incorporated into the crystal structure of the materials. Hashimoto et al. [25] have concluded that the incorporation of water in as-prepared $Ba_2In_2O_5$ is due to the absorption of water from the atmosphere and that this process did not affect the crystal

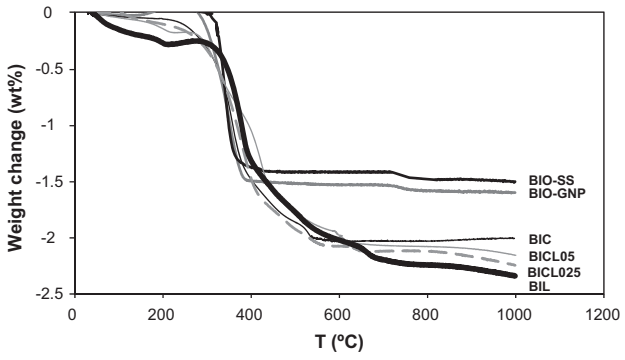

Fig. 5. TGA results for all compositions made by the GNP process and BIO made by the solid-state process. All experiments were performed in air, in the temperature range of 25–1000 °C with a heating rate of 5 °C min^{-1}.

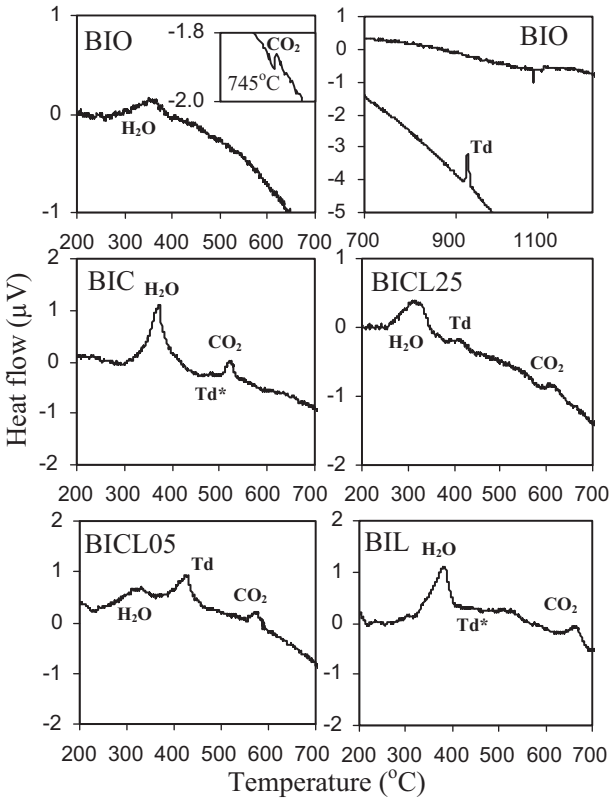

Fig. 6. DSC results for all compositions made by the GNP process. All experiments were performed in air, in the temperature range of 25–1000 °C with a heating rate of 5 °C min^{-1}.

structure of the material. As mentioned earlier, BIO sample prepared by the GNP method experienced a larger weight loss in this region, compared to the sample made by the solid-state method. This suggests higher accumulation of water in the grain boundary region than in the bulk material. Since other investigated compositions did not show difference between GNP and solid-state samples, it is possible that, in their case, water accumulates more in the bulk material. In addition, BIO samples, both the GNP and the solid-state, show smaller weight loss in this region, compared to all other compositions. Lower incorporation of water in the grain boundary area of the doped-$Ba_2In_2O_5$ is most likely related to the presence of Ce and La dopants in the $Ba_2In_2O_5$ structure and their higher segregation in the grain boundary region [27,28]. These dopants affect both the geometry of the structure (larger ionic radiuses of 0.87 Å Ce^{4+} and 1.03 Å for La^{3+}, compared to 0.8 Å for In^{3+}) [29] and the oxygen vacancy concentration in this area, both properties being related to the water incorporation in the materials [30], causing lower water content in the grain boundary area.

From Fig. 5 it is apparent that another smaller weight loss occurs at around 745 °C for BIO, 525 °C for BIC, 620 °C for BICL025, 580 °C for BICL05 and 660 °C for BIL. This is probably related to loss of CO_2, whose incorporation from air into the crystal structure of $Ba_2In_2O_5$ is also reported by Hashimoto et al. [25]. This process is also observed on the corresponding DSC curves as an endothermic peak, as shown in Fig. 6.

In addition to the H_2O and CO_2 losses, the TG and DSC results for all of the investigated materials revealed changes due to the order–disorder transition and change of oxygen stoichiometry. As discussed earlier, the temperature-profile XRD results for BIO, BIC, BICL025, BICL05, and BIL show phase changes between the ordered brownmillerite and disordered cubic perovskite structures. Based on these results it was expected that the associated characteristic

endothermic peaks on heating and exothermic peaks on cooling would be observed in the DSC for reversible order–disorder transition [23,31,32]. The endothermic peak was observed for the BIO sample at 925 °C on heating and the exothermic peak at 1090 °C on cooling, as shown in the DSC in the top right corner of Fig. 6. For BIC, BICL025, BICL05 and BIL samples the peaks related to this order–disorder transition could not be not easily distinguished. The temperatures associated with this change are close to the temperatures at which the materials lose water, and the thermal effects in some cases overlap. However, for most samples except BIC and BIL, small endothermic changes in DSC could still be detected.

A possible explanation for the thermal effects observed in the DSC curves is given by Yang and Lin [33]. The transition of oxygen vacancies from an ordered brownmillerite to a disordered cubic structure in perovskite-type oxides is accompanied by a change in oxygen content in the material (oxygen sorption). While the process of the structural transition is endothermic, oxygen sorption is an exothermic process. During the change from the brownmillerite to the cubic structure in our materials, a combined thermal effect is occurring. In the case of BIO, the endothermic effect of the phase transition is stronger than the exothermic effect of the oxygen sorption; hence the total heat effect is endothermic. In the case of BIC, BICL025, BICL05 and BIL, the heat spent during the phase transformation is similar to the heat released during oxygen sorption, and consequently the total heat effect is very small. In the corresponding TG scans all materials show a small weight increase (shown as a change of slope) due to the oxygen sorption, starting around the order–disorder transition temperatures. Based on the results obtained from the temperature-profile XRD, TGA and DSC we concluded that all the investigated materials undergo the order–disorder transition, accompanied with the increase in oxygen stoichiometry. The order–disorder transition temperatures were determined from the detected DSC peaks, or, in the case of BIC and BIL, estimated based on combined data from XRD, DSC and TGA. The temperatures are given in Table 3.

3.4. Conductivity measurements

The main goal for the conductivity tests was to compare electrical conductivity of the five different compositions and potentially determine a candidate material to act as a proton conductive electrolyte for an intermediate temperature fuel cell. It was anticipated that conductivity results in hydrogen-containing atmospheres would give us an insight into the proton conduction capability of the materials. In addition, earlier discussed properties of the investigated materials, such as order–disorder transition temperature and presence of the absorbed water in the structure, were correlated to the measured conductivities. The effect of the microstructure was also investigated by comparing the conductivity of samples made by the solid-state process (final grain size of the sintered pellets ~60 nm, determined by the Scherrer equation) and by the GNP process (final grain size of the sintered pellets ~40 nm, determined by the Scherrer equation and confirmed by TEM). Table 2 gives a summary of the properties of the samples used in the conductivity study. They all had final brownmillerite structure and sample porosity of about 20%. Fig. 7a–d shows SEM pictures of the polished and etched cross-sections of the sintered samples obtained by two different methods (GNP and the solid-state method). Fig. 7a

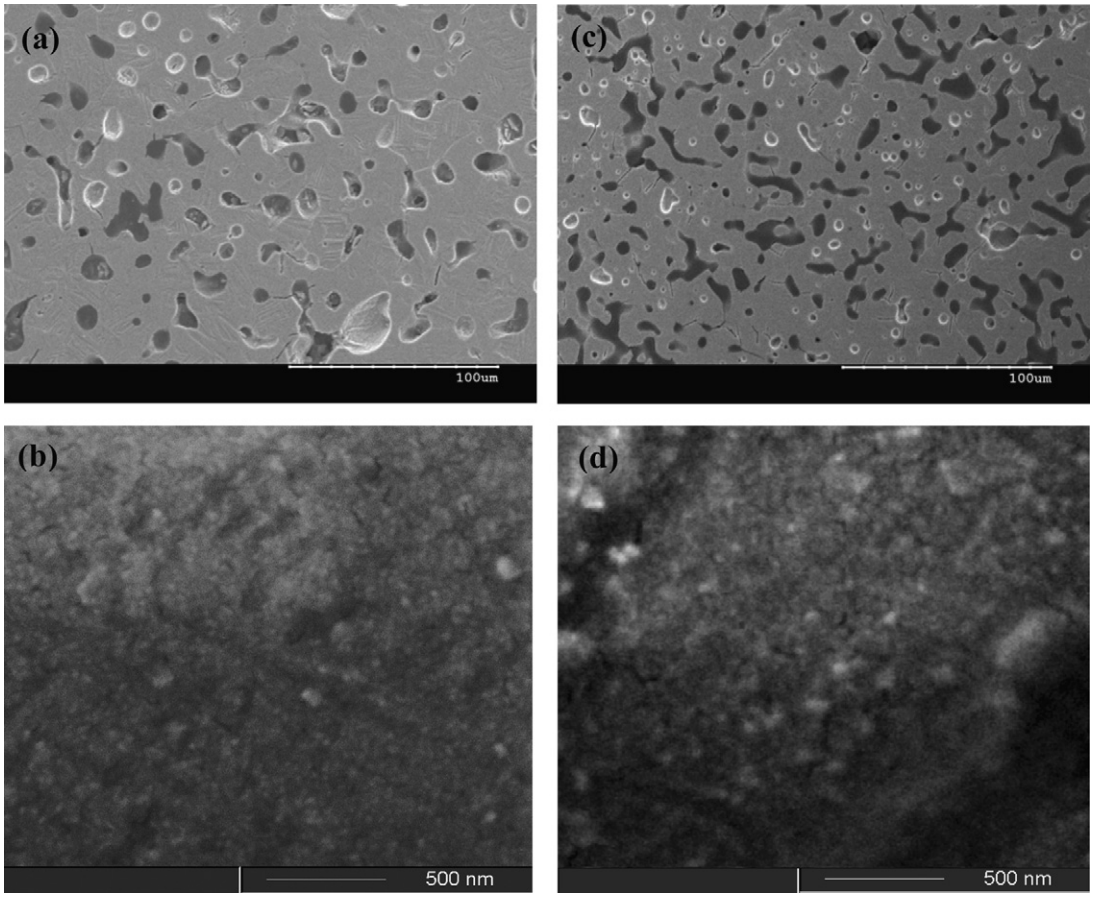

Fig. 7. SEM pictures of the polished and etched cross-sections of the sintered samples obtained by two different methods (GNP and the solid-state method): low (a) and high (b) magnification SEM picture of a GNP sample. The high resolution picture reveals grain sizes lower than ~50 nm; low (c) and high (d) magnification SEM picture of a SS sample. The high resolution picture for the SS sample reveals grain sizes between 60 and 80 nm.

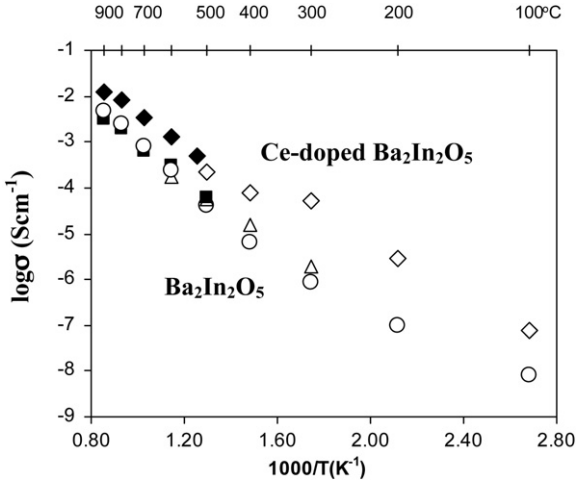

Fig. 8. Arrhenius plot of $Ba_2In_2O_5$ (BIO) and Ce-doped $Ba_2In_2O_5$ (BIC) conductivity in air: (○) BIO in this work; (■) BIO in Niwa et al. [18]; (△) BIO in Zhang and Smyth [11] (measured in wet air); (◊) BIC in this work; (♦) BIC in Niwa et al. [18].

and b shows the low (a) and high (b) magnification SEM picture of a GNP sample. The high resolution picture reveals smaller grain sizes (smaller than ~50 nm). Fig. 7c and d shows the low (c) and high (d) magnification SEM picture of a SS sample. The high resolution picture for the SS sample reveals larger grain sizes (between 60 and 80 nm). This confirms results obtained by the Scherrer formula.

Comparison of the electrical conductivity for all compositions (except for BICL05, which could not be successfully prepared) was done in both air and 50% hydrogen balanced by nitrogen. Fig. 8 shows Arrhenius plots of measured conductivity in air of a BIO and a BIC sample in this work made by the solid-state process, compared to some literature data. Comparable conductivities for the BIO sample were obtained. The somewhat lower conductivities of the BIO samples in this work are most likely due to the different conditions applied. Zhang and Smyth [11] measured conductivity in H_2O saturated air, while our measurements were performed in dried atmospheric air (moisture content 15 ppm). As reported by Zhang and Smyth, moisture in the air provides protonic conductivity in $Ba_2In_2O_5$, especially at temperatures below 500 °C, resulting in higher total conductivity. The conductivity of the BIC sample below 500 °C in our study seem to be a reasonable extension of data reported by Niwa et al. [18], which was only measured at temperatures above 500 °C (humidity not defined).

Fig. 9 compares conductivities in air (a) and 50% H_2/50% N_2 (b) for samples made by the solid-state process. Solid symbols in both graphs represent examples when as-prepared samples were tested. These samples contain absorbed water in the structure, as known from the TGA results. Hollow symbols show the conductivity results for the "dry" samples, which were heated to 380 °C for 3 h to release the water before the conductivity measurements. When measured in air, as-prepared BIO sample shows a sudden drop in conductivity between 300 °C and 400 °C. This is due to the release of water in this temperature range, as reported in our TGA results. As discussed earlier, water present in the structure provides protonic conduction and contributes to the total electrical conduction. Once the water leaves the structure, conductivity is mainly due to other charge carriers (ions and holes). When the "dry" BIO sample was tested, the total conductivity below 300 °C was lower than for the as-prepared sample, and was linearly increasing with the temperature. The higher conductivity below 300 °C for the as-prepared sample reveals that the water present in the sample provides a significant protonic contribution to the total conductivity. On the other hand, as shown for the case of BIC in Fig. 9a, as-prepared BIC, BICL025, and BIL samples did not show a significant change in conductivity in air due to release of water from the structure, neither they showed a significant difference between the as-prepared and the "dry" samples. Contribution to the total conductivity provided by the absorbed water is much smaller for these compositions than for the BIO sample. This is opposite to what was expected, since TGA results showed that BIC, BICL025, and BIL have a higher content of water present in the structure, compared to BIO. However, the TGA suggested also that, for these materials, water accumulates more in the bulk, while for BIO its accumulation is higher in the grain boundary. Hence, stronger effect of water on the conductivity of BIO suggests that grain boundary plays a more important role in proton conductivity provided by water than bulk of the materials.

When all "dry" samples were compared in air, the conductivity of the BIC sample was the highest, while BICL025 and BIL samples have the lowest conductivities. For these three compositions there is a decrease in the conductivity around 400 °C. Since the effect of water is eliminated by heating the materials before testing, this change in conductivity can be related only to the order–disorder transition, confirmed earlier by the temperature-profile XRD and the DSC tests. This structure transition and loss of oxygen vacancies due to the associated oxygen sorption is most likely causing the loss of conductivity. It is interesting to notice that BIO and BIC show similar activation energy of ionic conduction of about 0.64 eV and 0.61 eV respectively, while BICL025 and BIL have a

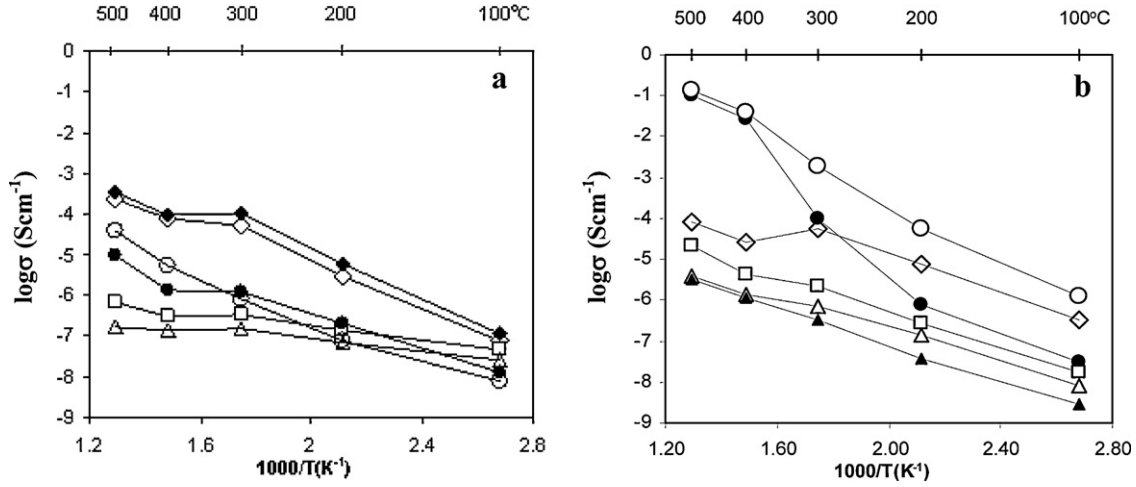

Fig. 9. Electrical conductivity in (a) air and (b) H_2/N_2 for solid-state samples: as-prepared samples: (●) BIO, (♦) BIC, (▲) BIL; "dry" samples: (○) BIO, (◊) BIC, (□) BICL025, (△) BIL.

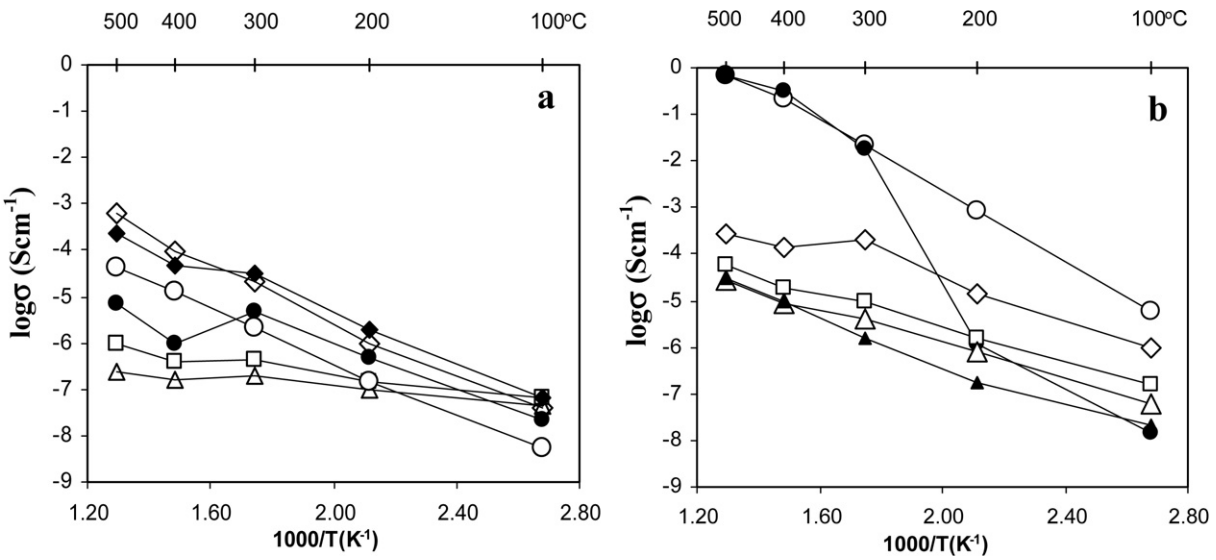

Fig. 10. Electrical conductivity in (a) air and (b) H_2/N_2 for GNP samples: as-prepared samples: (●) BIO, (♦) BIC, (▲)BIL; "dry" samples: (○) BIO, (◊) BIC, (□) BICL025, (△) BIL.

lower activation energy of about 0.18 eV, suggesting differences in conduction mechanisms for these two groups of materials.

All measured conductivities for "dry" samples were reversible with cycling (heating and cooling between 100 °C and 500 °C). As-prepared samples, after the initial loss of conductivity due to water release during heating, achieved the same conductivities as the "dry" samples during cooling. The values were reversible with cycling, as well. This was also true for the GNP samples, discussed later.

Fig. 9b shows the conductivities measured in the hydrogen-containing atmosphere for the solid-state samples. Again, for the as-prepared BIO sample, an effect of water was noticed, in this case as a sharp increase in conductivity. When present, water in the structure is in interaction with the oxygen vacancies and oxygen ions [12,34]. When water is released, hydrogen incorporates directly and interacts with the free oxygen vacancies and ions, significantly improving conductivity. The mechanisms are suggested in the literature [12–14,34]. The decomposition or reduction of the material were excluded as possible causes for increased conductivity, as no changes in composition or structure were observed by XRD after the test in hydrogen. When the temperature was reduced during the testing, the achieved conductivities were higher than in the heating stage and the same as for the "dry" samples. When conductivity was measured for the "dry" BIO sample, a linear increase in conductivity was recorded, with two orders of magnitude higher conductivities at temperatures below 300 °C, compared to the as-prepared sample. This high conductivity is most likely due to the direct incorporation of hydrogen into the structure and suggests a possible high contribution of protonic conductivity in BIO in the presence of hydrogen. Similar, but much less enhanced effect of water was found for as-prepared BIC, BICL025, and BIL samples. When all "dry" samples were tested in hydrogen, their conductivities were higher than conductivities in air for all compositions, except BIC whose conductivity was lower. All composition showed similar energy of activation of 0.45 eV, revealing the same mechanism of conduction in hydrogen. "Dry" BIC, BICL025 and BIL showed a small change in slope at 400 °C with decrease in the conductivity, which is, again, due to the transformation from the brownmillerite to the cubic structure. Even more, BIC, BICL025, and BIL samples retained this cubic structure after the testing in hydrogen, as confirmed by X-ray diffraction.

Fig. 10 shows a comparison between conductivity in air (a) and 50% H_2/50% N_2 (b) for samples made by the GNP process. The effect of water on the conductivity of the as-prepared samples in both atmospheres was similar to the solid-state samples, but much more enhanced for the BIO-GNP sample, especially in hydrogen. When "dry" GNP samples were measured in air, the measured conductivities were very similar to the conductivities for the solid-state samples. The change in conductivity in air due to the order–disorder transition is again present for BIC, BICL025, and BIL. In hydrogen-containing atmospheres, the improvement in conductivity compared to the tests in air is much more enhanced for the GNP samples. In this atmosphere, changes in conductivity due to the order–disorder transition for the BIC, BICL025, and BIL samples were noticed around 400 °C, as for the solid-state samples. Surprisingly high conductivities between 0.02 S cm^{-1} and 0.7 S cm^{-1} were obtained for $Ba_2In_2O_5$ sample in the temperature range from 300 °C to 500 °C.

In order to investigate the effect of the grain size/grain boundary on the electrical properties of the materials, the conductivities of the GNP samples were compared to the solid-state samples in air (Figs. 9a and 10a) and in hydrogen-containing atmosphere (Figs. 9b and 10b). GNP samples, with the smaller grain size and, hence, larger grain boundary area are expected to show higher effect of the grain boundary. When measured in air, the conductivity results were very similar for the GNP and the solid-state samples. This suggests that grain boundary does not play a significant role in conductivity of oxygen ions and holes, at least not in this temperature range. Fig. 11a shows an example of the AC impedance spectra for BIO measured in air at 400 °C, comparing spectra recorded for the GNP and the solid-state samples. Although grain boundary contribution to the impedance could not be distinguished from the bulk contribution, a small decrease in total impedance for the GNP sample is most likely due to the effects of the grain boundary (since bulk contribution is a property of the material and does not change with the microstructure). However, no significant effect of the grain size is noticed in air. It is possible that a stronger effects would be noticed at higher temperatures (>500 °C), when the mobility of oxygen ions is higher. On the other hand, it is apparent that the sample preparation method and associated microstructure does have an effect on the conductivity in hydrogen, showing conductivities an order of magnitude higher for the GNP samples. The effect is especially enhanced for the BIO sample. Effect of water and its contribution to the total conductivity is also more enhanced for the BIO sample prepared by the GNP method. In the literature [11,12,34] it is anticipated that

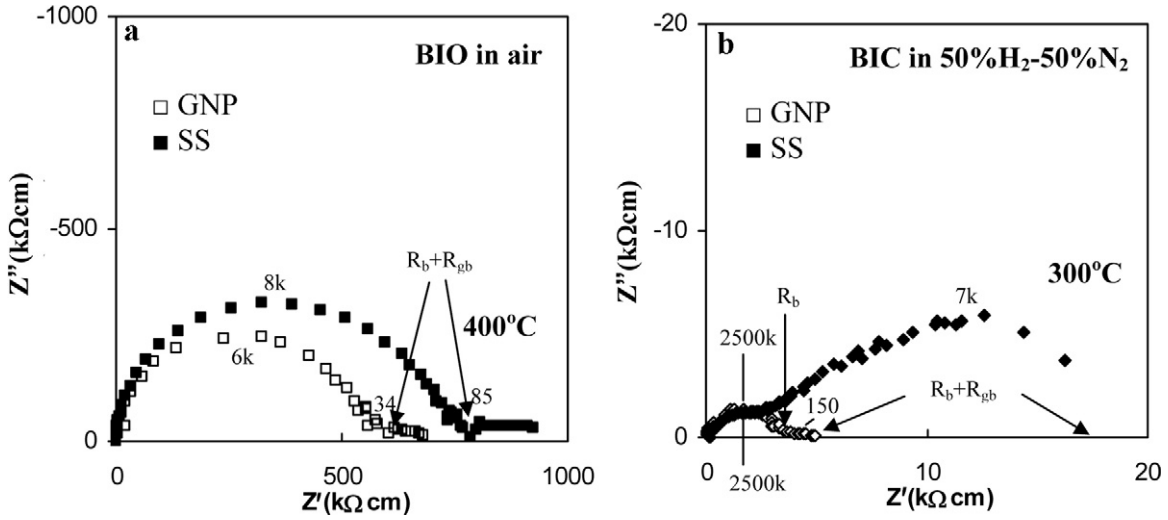

Fig. 11. AC impedance scans for: (a) BIO-GNP samples (grain size ~ 40 nm) and BIO-SS samples (grain size ~ 60 nm) measured in air; (b) BIC-GNP samples (grain size ~40 nm) and BIC-SS samples (grain size ~60 nm) measured in H_2/N_2. Characteristic frequencies are given in Hz. Arrows show the locations where the bulk (R_b) and the total material resistances ($R_b + R_{gb}$) were taken.

this conductivity in hydrogen and humidity is mainly due to the proton conductivity. Therefore, our results suggest that the grain boundary plays an important role in the conduction mechanism of protons, possibly by having a higher concentration of oxygen vacancies in this region. Easily accessible oxygen vacancies enable oxygen ion incorporation in air, and proton incorporation in water or hydrogen. In addition, higher concentration of oxygen vacancies improves charge transport along the grain boundaries. The process is enhanced in hydrogen atmospheres, as the mobility of protons is superior at the low temperatures, compared to oxygen ion mobility. As an example of the strong grain boundary effect in hydrogen, Fig. 11b shows significantly lower grain boundary impedance for the GNP samples compared to the solid-state samples. A detailed study of the effect of atmosphere, dopant, grain boundary and the mechanism of proton conduction in $Ba_2In_2O_5$ based materials is reported in our other publication [35].

From the conductivity measurements in hydrogen-containing atmospheres for all prepared samples, undoped $Ba_2In_2O_5$ prepared by the glycine-nitrate method could be selected as a potential material for application as an intermediate temperature electrolyte. A more detailed study of $Ba_2In_2O_5$ conductivity in hydrogen-containing atmospheres with determined proton transport number has been reported in our other work [30].

4. Conclusions

Five different compositions of undoped and Ce- and La-doped $Ba_2In_2O_5$ were successfully synthesized by the solid-state process and the glycine-nitrate process. The orthorhombic brownmillerite structure was achieved for all compositions in the lower temperature range of 1100 to 1400 °C, while the cubic perovskite structure was achieved for all materials at 1500 °C, except for BIL, which achieved this structure already at 1300 °C. In the case of powders produced by the glycine-nitrate process, the grain size, determined by the powder X-ray diffraction, increased from the initial ~10 nm to ~70 nm with the sintering temperature of 1500 °C. In the case of the powders prepared by the solid-state process, produced powders had an initial grain size of ~40 nm, which increased to ~80 nm with heating to 1500 °C. Stability studies for all five compositions demonstrated that these compositions are not stable in highly humid atmospheres with RH = 90% up to 70 °C over 24 h, while higher stability was observed for RH = 50%. All materials showed stability in 3% mol steam in air flow up to 500 °C for at least 24 h.

Temperature profile X-ray diffraction revealed that all powders undergo a phase transformation with heating between 400 °C and 1000 °C. This transformation is related to the order–disorder transformation, when an ordered brownmillerite structure changes to a disordered cubic structure and vice versa. DSC tests also confirm this change, although, except for BIO, distinguished peaks associated with this order–disorder transition were hard to observe. Oxygen sorption associated with the order–disorder transition was observed in the TGA curves, showing a small weight gain during the change to a cubic structure. Ce- and La-doped $Ba_2In_2O_5$ experienced this transformation at lower temperatures compared to undoped $Ba_2In_2O_5$, which confirmed the initial hypothesis in this work. TGA results also showed two processes that take place below 1000 °C with heating: release of H_2O and CO_2 from the crystal structure. Conductivity tests for BIO, BIC, BICL025 and BIL samples, prepared by both the glycine-nitrate process and solid-state reaction, were performed in air and hydrogen containing atmospheres.

Conductivity results revealed that the conductivity of these materials is affected by their properties (water content and order–disorder transition), dopant, microstructure, and atmosphere. Samples made by the glycine-nitrate process, with resulting smaller grain size of about 40 nm and larger grain boundary area, showed higher conductivity in hydrogen than samples produced by the solid-state reaction with a grain size of about 60 nm. These results revealed that the grain boundary plays an important role in the proton conduction mechanism. On the other hand, there was no significant difference in conductivity in air between the GNP samples and the solid-state samples. All compositions showed higher conductivity in a hydrogen atmosphere than in oxygen, especially the GNP samples. Compared to Ce- and La-doped $Ba_2In_2O_5$, undoped $Ba_2In_2O_5$ showed several orders of magnitude higher conductivity in hydrogen containing atmosphere at temperatures between 300 °C and 500 °C, especially the samples produced by the glycine-nitrate process (conductivity between 0.02 S cm^{-1} and 0.7 S cm^{-1}).

Based on the results, undoped $Ba_2In_2O_5$ produced by the glycine-nitrate process is the most promising material from the investigated group for further proton conductivity investigation. Although conductivity results in hydrogen-containing atmospheres give us an indication of proton conductivity, it is

crucial to accurately determine the contribution of proton conduction in the total conductivity measured. This has been investigated and reported in another paper. Also, additional optimization of sample preparation, sintering and densification of the pellet, as well as improving the stability of the material in humid atmospheres (possibly by investigating new doping elements) is needed if this material is to be used as an electrolyte material in intermediate temperature fuel cells.

Acknowledgements

Financial support from the Natural Sciences and Engineering Research Council of Canada (NSERC) for this project is gratefully acknowledged. The authors thank the National Research Council-Institute for Fuel Cell Innovation (NRC-IFCI) and Northwest Mettech Corp. for support of this project.

References

[1] M.K. Debe, S.J. Hamrock, R.T. Atanasoski, IV.A.3 Advanced MEAs for Enhanced Operating Conditions, DOE Hydrogen Program FY 2004 Progress Report.
[2] M.K. Debe, S.J. Hamrock, R.T. Atanasoski, Fuel Cell (2004).
[3] R.T. Atanasoski, IV.C.5 Novel Approach to Non-Precious Metal Catalysts, DOE Hydrogen Program FY 2004 Progress Report.
[4] Y. Song, Y. Wei, H. Xu, M. Williams, Y. Liu, L.J. Bonville, et al., J. Power Sources 141 (2005) 250–257.
[5] P. Jannasch, Curr. Opin. Colloid Interface Sci. 8 (2003) 96–102.
[6] G. Alberti, M. Casciola, Solid State Ionics 145 (2001) 3–16.
[7] B. Wang, J. Power Sources 152 (2005) 1–15.
[8] B.R. Limoges, R.J. Stanis, J.A. Turner, A.M. Herring, Electrochim. Acta 50 (2005) 1169–1179.
[9] T. Norby, Solid State Ionics 125 (1999) 1–11.
[10] C.A.J. Fisher, M.S. Islam, Solid State Ionics 118 (1999) 355–363.
[11] G.B. Zhang, D.M. Smyth, Solid State Ionics 82 (1995) 161–172.
[12] R. Hui, R. Maric, C. Decès-Petit, E. Styles, W. Qua, X. Zhang, et al., J. Power Sources 161 (2006) 40–46.
[13] N. Bonanos, Solid State Ionics 53–56 (1992) 967–974.
[14] T. Schober, J. Friedrich, Solid State Ionics 113–115 (1998) 369–375.
[15] M. Karlsson, A. Matic, C.S. Knee, I. Ahmed, S.G. Eriksson, L. Börjesson, Chem. Mater. 20 (2008) 3480–3486.
[16] C.A.J. Fisher, M.S. Islam, R.J. Brook, J. Solid State Chem. 128 (1997) 137–141.
[17] Q. Yin, Y.S. Lin, Solid State Ionics 178 (2007) 83–89.
[18] J. Niwa, T. Suehiro, K. Kishi, S. Ikeda, M. Maeda, J. Mater. Sci. 38 (2003) 3791–3795.
[19] J.B. Goodnough, J.E. Ruiz-Daiz, Y.S. Zhen, Solid State Ionics 44 (1990) 2l–31l.
[20] K. Kakinuma, H. Yamamura, H. Haneda, T. Atake, Solid State Ionics 140 (2001) 301–306.
[21] T. Mitamura, H. Ogino, H. Kobayashi, J. Am. Ceram. Soc. 76 (8) (1993) 2127–2128.
[22] B.D. Cullity, S.R. Stock, Elements of X-ray Diffraction, 3rd ed., Prentice-Hall Inc., 2001, pp. 167–171.
[23] T. Hashimoto, Y. Ueda, M. Yoshinaga, K. Komazaki, K. Asaoka, S. Wang, J. Electrochem. Soc. 149 (10) (2002) A1381–A1384.
[24] H. Yamamura, Y. Yamada, T. Mori, T. Atake, Solid State Ionics 108 (1998) 377–381.
[25] T. Hashimoto, Y. Inagaki, A. Kishi, M. Dokiya, Solid State Ionics 128 (2000) 227–231.
[26] T. Schober, Solid State Ionics 99 (1997) 9–13.
[27] S.B. Desu, D.B. Payne, J. Am. Ceram. Soc. 73 (11) (1990) 3391–3397.
[28] S.B. Desu, D.B. Payne, J. Am. Ceram. Soc. 3 (11) (1990) 3398–3406.
[29] N.N. Greenwood, A. Earnshaw, Chemistry of the Elements, 2nd ed., Butterworth-Heinemann, an imprint of Elsevier Science, 1997, p. 1295.
[30] W. Fischer, G. Reck, T. Schober, Solid State Ionics 116 (1999) 211–215.
[31] Q. Yin, Y.S. Lin, Adsorption 12 (2006) 329–338.
[32] S. McIntosh, J.F. Vente, W.G. Haije, D.H.A. Blank, H.J.M. Bouwmeester, Solid State Ionics 177 (2006) 1737–1742.
[33] Z.H. Yang, Y.S. Lin, Solid State Ionics 176 (2005) 89–96.
[34] J. Jankovic, D.P. Wilkinson, R. Hui, J. Electrochem. Soc. 158 (1) (2011) B61–B68.
[35] J. Jankovic, D.P. Wilkinson, R. Hui, J. Electrochem. Soc. 159 (2) (2011) B1–B12.